

TIME-RESOLVED RECONSTRUCTION OF SUPER-STREAKS IN HIGH REYNOLDS NUMBER TURBULENT BOUNDARY LAYER OVER A FLAT PLATE

S. Roux¹, F. Kerhervé², J.M. Foucaut², M. Stanislas², J. Delville³

¹ Laboratoire de Thermocinétique de Nantes UMR 6607, Université de Nantes (France)

² Laboratoire de Mécanique de Lille, UMR CNRS 8107, EC-Lille, Univ. Lille 1 (France)

³ Institut PPRIME, CNRS UPR 3346, Université de Poitiers, ENSMA, France

ABSTRACT

A methodology for examination of *super-structures* in a zero pressure gradient boundary layer at Reynolds number of 10000 is presented. These structures are characterised by a large degree of persistence and are thought to participate actively to the turbulence regeneration in near-wall region (Mathis *et al.*, 2011). A time-resolved estimate of the three-dimensional structure of these entities is obtained by combining low-speed two-dimensional stereo-PIV (Particle Image Velocimetry) and a two-dimensional rake of 143 single hot-wire probes. The latter is used to animate the PIV data, initially sampled at 4Hz, at a higher sampling rate. This is effected using linear stochastic estimation (LSE) with a multi-time delay formulation. The potential of the methodology for eduction of the very large low-speed streaks and the associated hairpin vortices is discussed.

Introduction

Evidence of identifiable structures in turbulent boundary layers was brought from intensive studies in the last decades. Initially, academic research focused mostly on the near-wall region, allowing taxonomy of structures to be obtained with large consensus for low to moderate Reynolds numbers (Robinson, 1991), among which the near-wall streaks (Smith & Metzler, 1983; Hamilton *et al.*, 1995) or associated hairpin vortices (Theodorsen, 1952; Adrian & Moin, 1988; Christensen & Adrian, 2001). A well-established robust feature is the streaky structure initially described by Kline *et al.* (1967) from bubble visualisations. This is thought to play an essential role in the turbulent self-sustained mechanism in the near-wall region (Stanislas *et al.*, 2008). At higher Reynolds numbers, accurate turbulence measurements becomes increasingly difficult. The near-wall boundary layer structure and the role of the underlying flow features become more controversial (Smits *et al.*, 2011). Further from the wall in the so-called log-region, flow visualisations (Tomkins & Adrian, 2003) and multi-point measurements (Blackwelder & Kovaszny, 1972) put evidences of dominant structures with again identifiable patterns but with dimensions of an order of magnitude greater than their near-wall twins. These are usually referred as *very large scale motions* or *super-structures*. Their existence was initially postulated by Townsend (1976) by introducing the concept of *inactive motion* to explain the Reynolds-number dependence of turbulence quantities and the absence of full similarity over the entire boundary layer

section. These *inactive motions* have been first interpreted as large eddies which can contribute to the shear stress at large distances from the wall but not in the inner layer.

There is now strong evidences that these entities play a crucial role in the near-wall flow dynamics where most of turbulence is generated (Smits *et al.*, 2011). They are thought to be responsible for the amplitude-modulation of the inner-region (Mathis *et al.*, 2011) by imposing their signatures and therefore playing an active role in the near-wall regeneration. Eduction and complete characterisation of these structures in high Reynolds turbulent boundary layers remains experimentally and numerically not a simple task although nowadays numerical simulations can reach high enough Reynolds numbers to be nearly free from low Reynolds number effect. Adrian *et al.* (2000) offered a detailed description of the these structures as well as a conceptual scenario for their organisation at moderate Reynolds numbers. At high Reynolds numbers, the large scale structures are embedded into a very wide range of scales distributed from Kolmogorov microscale to the boundary layer thickness. This makes their eduction not easily manageable. To quantify this wide range of scales, Sirovich (1989) suggests that the number of degree of freedom of the flow dynamics is of order of $Re^{9/4}$, where Re denotes the Reynolds number. Even if this number is possibly far less in most flows, it is manifest that strategies to reduce the overall flow to its essential dominant features is necessary. Classical multi-point or multi-time statistics such as correlations have been used in the past to characterise super-structures in boundary layers (Kovaszny *et al.*, 1970; Blackwelder & Kaplan, 1976; Tutkun *et al.*, 2009a). These remains however limited and do not allow a complete eduction. Due to the extremely long streamwise extend of the structures, velocity flow field measurements over a large region with high spatial resolution are needed. Even with the more advanced PIV system this remains most of the time unaffordable. Similarly, time-resolved spatially sparse multi-point measurements used alone also offer a limited description of these structures while the time-resolve description is necessary to follow the entire dynamics of the structures. Accurate eduction of these very large scale motions in the log-region requires thus both time- and spatially-resolved description of the flow field. None of the today experimental techniques or numerical capabilities can *alone* answer this challenging task. An alternative is therefore to take advantages of the different available experimental tools and recent mathematical developments in order to reconstruct the

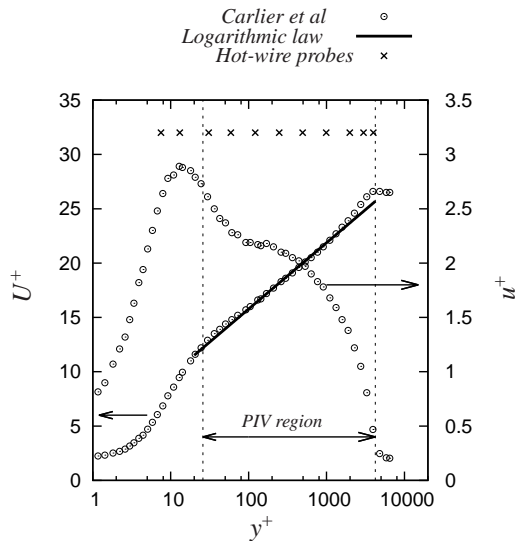


Figure 1. Mean & RMS velocity profiles obtained by Carlier & Stanislas (2005). The region of the boundary layer in the wall-normal direction covered in the current paper is represented by the vertical dashed line. The (\times) denotes the location of the probes along a given comb.

space-time evolution of these super-structures.

To attain such an objective, we here combine highly spatially resolved stereo-PIV measurements and multi-point time-resolved velocity measurements obtained using a two-dimensional rake of hot-wire probes. The linear stochastic estimation (LSE) is used to compute a set of estimates of the velocity field in the the two-dimensional PIV plane with similar spatial resolution than that of the PIV and similar time resolution than that of the hot-wire measurements. While the LSE does not provide a model of the flow physics it has been shown to capture the essential features of the flow that are most correlated with given events (Adrian, 1994). It thus offers a way to reduce the number of degree of freedom of the entire flow dynamics allowing manageable interpretation and eduction of flow mechanisms. In the meantime, it offers the possibility to estimate time-resolved velocity field from temporally sparse fields such as obtained by PIV data.

Flow configuration & Experimental set-up

The flow examined is a zero-pressure gradient turbulent boundary layer. The data are taken from the joined experimental campaign conducted during the European WALLTURB program in the large wind tunnel at Laboratoire de Mécanique de Lille (LML). Details of the wind tunnel can be found in Carlier & Stanislas (2005). The reader is referred to Stanislas *et al.* (2009) for complete details of the overall WALLTURB program.

The free-stream velocity is 5 m/s. Extensive description of the main flow properties (first and higher order moments profiles) has been provided in Foucaut *et al.* (2010); Coudert *et al.* (2011). Only the mean and RMS profiles in the cross-section of investigation are here given in figure 1(a). With usual notations, the y coordinates denotes the distance from the wall, z the distance in the spanwise direction, and x the main flow direction. Superscript $+$ denotes wall-unit normalisation. At the investigated position, the boundary layer thickness is 288 mm and the Reynolds num-

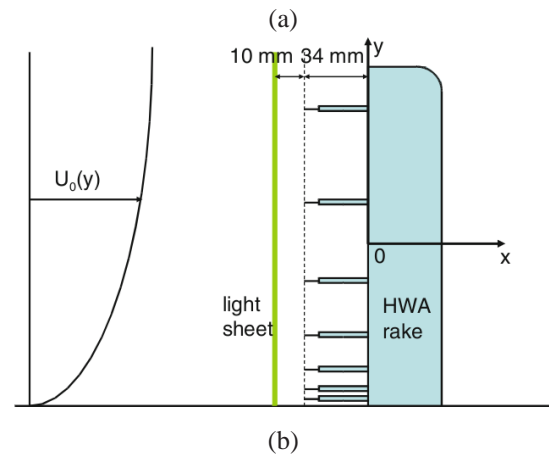
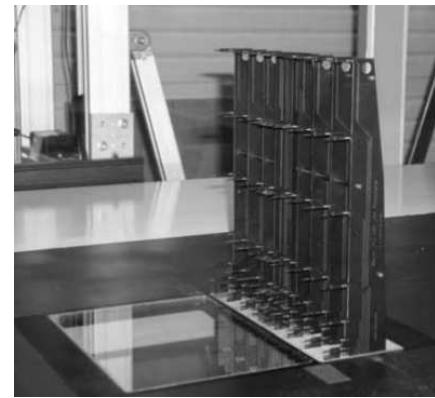


Figure 2. (a) View of the 143 hot-wires rake installed in the wind tunnel. (b) Sketch of the hot-wire rake showing the logarithmic distribution of the probes in the wall-normal direction and the rake location relative to the SPIV measurement plane.

ber Re_θ based on the momentum thickness is 9830. From previous experiments, the friction velocity u_τ was estimated to be 0.188 m/s.

The two-dimensional hot-wire rake, shown in figure 2(a), was designed and manufactured by the Institut PPRIME (Poitiers, France). It is made of a total of $N_h = 143$ single wire probes located in a $y-z$ plane normal to the flow and distributed over 13 combs in the spanwise direction each made of 11 probes separated logarithmically in both spanwise and wall-normal directions as shown in figure 2(b). The sensing wires are 0.5 mm long and 0.25 μm in diameter (11.8 and 0.006 respectively in wall units). The first and last rows of probes are located 0.4 mm and 306.9 mm respectively from the wall (corresponding to 7 and 7365 wall-units respectively). More details on the anemometry system and the calibration procedure can be found in Delville *et al.* (2010) and Coudert *et al.* (2011). For the present purpose, 534 blocks of 6s-long signals at a sampling frequency of $f_s = 30$ kHz (corresponding to a sampling interval $\Delta t^+ = u_\tau^2 / (f_s \nu) \approx 0.29$ with ν the kinematic viscosity) are considered.

In combination, a stereo PIV (SPIV) system, fully detailed in Coudert *et al.* (2011), is used to obtained the three components, spatially resolved, of the velocity field at a low repetition rate of 4Hz. The SPIV and hot-wire rake systems are synchronised using an external clock. The SPIV covers a $30 \times 30 \text{ cm}^2$ region parallel to the hot-wire rake (covering the entire boundary layer thickness) and located 1cm (or

240 wall units) upstream of the hot-wire rake as illustrated in figure 2(b). The spatial resolution of the final velocity field in both normal and spanwise directions is 2mm (or 48 wall units).

As shown in figure 2(a), the first two rows of the hot-wires rake are located below the PIV plane. For this reason, the corresponding hot-wires are not considered for the reconstruction method detailed further.

As discussed by Tutkun *et al.* (2009b), a blockage effect on the incoming boundary layer due to the hot-wire rake has been observed and rigorously quantified. This was found to be a potential effect with only little modification of the boundary layer turbulence structure.

Linear Stochastic Estimation

Time-resolved reconstruction of the three components of the velocity in the PIV plane with the same spatial resolution than that of the original PIV field is obtained using the linear stochastic estimation technique. By this means a linear approximation can be obtained for the conditional estimate of some quantity evaluated at point \mathbf{x} and time t given a set of observables evaluated at points $\mathbf{x}' = \{\mathbf{x}'_1, \dots, \mathbf{x}'_{N'}\}$ and times t' . In the present problem, the quantity to evaluate comprises the three components of the velocity $\mathbf{u}_{\text{piv}} = \{u_1, u_2, u_3\}(\mathbf{x}, t)$ in the PIV plane, while the set of observables is the longitudinal velocity component $u^h(\mathbf{x}', t')$ measured at the N_h hot-wire probes. A multi-time formulation for the linear approximation of the velocity component $u_i(\mathbf{x}, t)$ is used, such as used by Kerhervé *et al.* (2012). This can be written as follows,

$$\hat{u}_i(\mathbf{x}, t') = \sum_{k=1}^{N_h} a_{i,k}(\mathbf{x}) u^h(\mathbf{x}'_k, t' + \tau(\mathbf{x}, \mathbf{x}'_k)) \quad i = 1, 2, 3 \quad (1)$$

where $a_{i,k}(\mathbf{x})$ denotes the unknown coefficient matrix relating the conditional field and the observers, and $\tau(\mathbf{x}, \mathbf{x}')$ a time-delay evaluated between a point \mathbf{x} in the PIV plane and hot-wire sensor \mathbf{x}' . The coefficients are obtained by solving, for each point \mathbf{x} of the PIV grid and for each i -th velocity component, a linear system of equations of the form $\mathbf{A}\mathbf{y}_i = \mathbf{b}_i$ ($i=1,2,3$), where $\mathbf{A} \in \mathbb{R}^{N_h \times N_h}$, $\mathbf{y}_i \in \mathbb{R}^{N_h}$, $\mathbf{b}_i \in \mathbb{R}^{N_h}$ – detailed expression may be found in Kerhervé *et al.* (2012) – related to two-point correlations at specific time delays between conditional events and the observers.

The time delays $\tau(\mathbf{x}, \mathbf{x}')$ are defined as the retarded time at which the maximum of correlations between PIV point \mathbf{x} and HWA sensor \mathbf{x}' calculated for the longitudinal velocity fluctuations occurs. The same time delays have been used for the conditional estimate of the normal and spanwise velocity components. This choice is discussed below.

Due to measurement errors, the linear system $\mathbf{A}\mathbf{y}_i = \mathbf{b}_i$ is generally badly conditioned such that its resolution by a direct calculation of the inverse of \mathbf{A} would result in diverging solution for $\hat{u}_i(\mathbf{x}, t')$. The regularisation procedure suggested by Cordier *et al.* (2010) and further applied by Kerhervé *et al.* (2012) is here implemented. The solution \mathbf{y}_i of the system is calculated via a filtering of the singular elements of the matrix \mathbf{A} following the Tikhonov regularisation procedure.

Results

Evaluation of the quality of the estimate

The methodology described above is applied independently for each of the three components of the velocity in the PIV region. The hot-wire time-series are disseminated such that the reconstruction is effected at a sampling frequency of 1.5 kHz. Time histories of the conditional estimate $\hat{u}_i(\mathbf{x}, t)$ at a selection of points closest to that of the selected hot-wire sensors, are shown in figure 3. For each time series reported here, the overall temporal dynamic is well reproduced by the conditional estimate. While not shown clearly in the figure, some slight time delay between the conditional estimate and the hot-wire signal is noted. This time delay corresponds to the separation distance between the PIV plane and the hot-wire rake and depends on the local convection velocity. A low-pass filtering of the original data is somewhat observed, leading to a loss of energy in the reconstructed signal such as depicted in figure 4(b) where levels of $u^+ = (u'^2)^{1/2}/u_\tau$ are reported. Due to the logarithmic spacing of the hot-wire sensors, both in the spanwise and normal directions, the loss of fluctuating energy is amplified for points in the PIV region located between the hot-wire probes. However, for these points, the continuity of the local dynamic is well conserved as illustrated in figure 3 where time histories of the conditional estimate at two PIV points located half way of two successive hot-wire sensors in the normal direction are reported. The loss of energy is in agreement with the observations made when examining the PIV/HWA correlation coefficients, since the reconstructed energy is directly linked to the level of correlation between the conditional variables and the observers. *The loss of fluctuating energy must not be seen neither as an error nor a loss of information:* it represents a reduction of the order of complexity of the original data, the initial objective of the proposed methodology. To avoid the non-homogeneous distribution of the turbulence energy of the conditional field in the spanwise direction, the original hot-wire velocity signals could have been first decomposed into Fourier and POD modes in the spanwise and wall-normal directions respectively. This may constitute a perspective of the presented work but not the present objective.

To better quantify the order-reduction effect discussed above, the spectral content of the conditional field is examined. Figure 3(b) compares energy spectra of the streamwise velocity component at selected points of the conditional estimated field with that obtained from hot-wire time signals. The spectra are averaged over the spanwise direction. The low-frequency filtering is manifest close to the wall: as discussed above the most correlated events correspond to the largest scales of the flow well characterised by low wavenumbers. The LSE procedure therefore implies a filtering of the lowest correlated events and leads here to an eduction procedure of the scales remaining the most correlated between the PIV field and the plan formed by the hot-wire rake, the largest scales of the flow (not necessarily the most energetic ones) in which we are interested in.

Identification of very large low-speed streaks

A snapshot of the original PIV fluctuating velocity field in the (y, z) plane is reported in figure 5(a). The streamwise component is shown as colormap while the vectors give the spanwise and wall-normal fluctuating components. The snapshot exhibits an expected complex dynamics embedding low and large energetic events in a wide range of

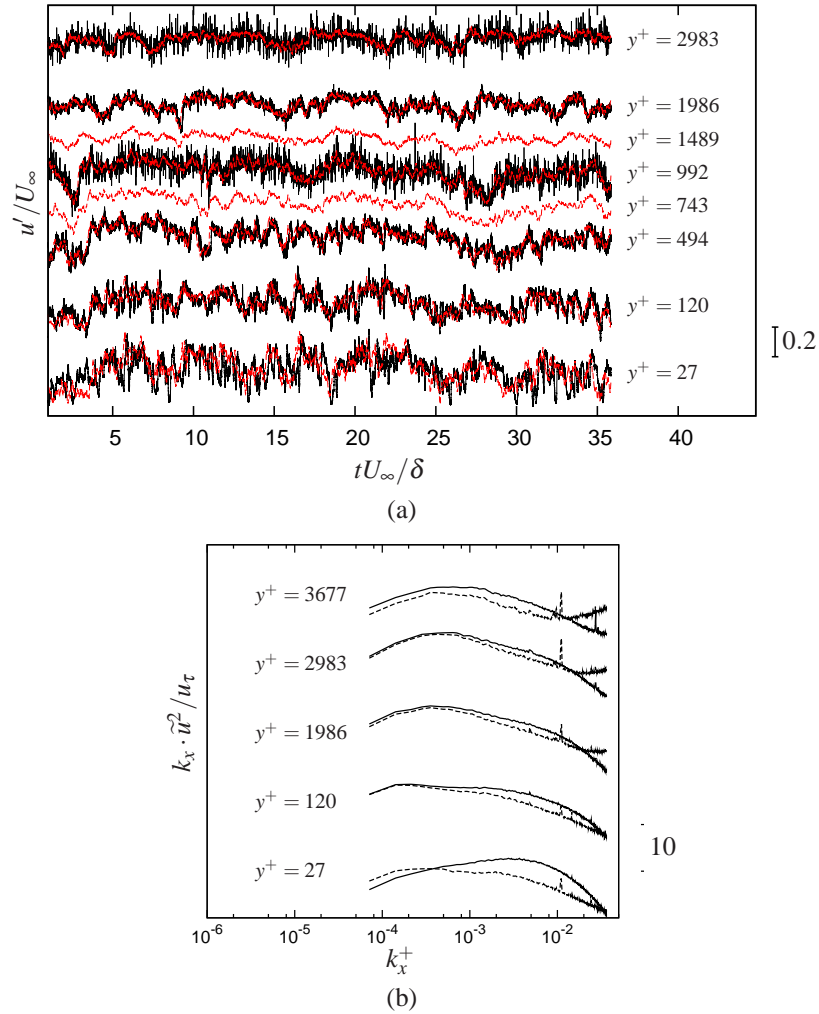


Figure 3. (a) Selection of time series of (dashed line) conditional estimated longitudinal velocity fluctuations compared with that of (line) nearest hot-wire sensor. (b) Frequency spectra of (dashed line) the conditional estimated longitudinal velocity fluctuations compared with (line) that obtained from hot-wire measurements. The PIV points are selected as the nearest from that of the hot-wire sensors.

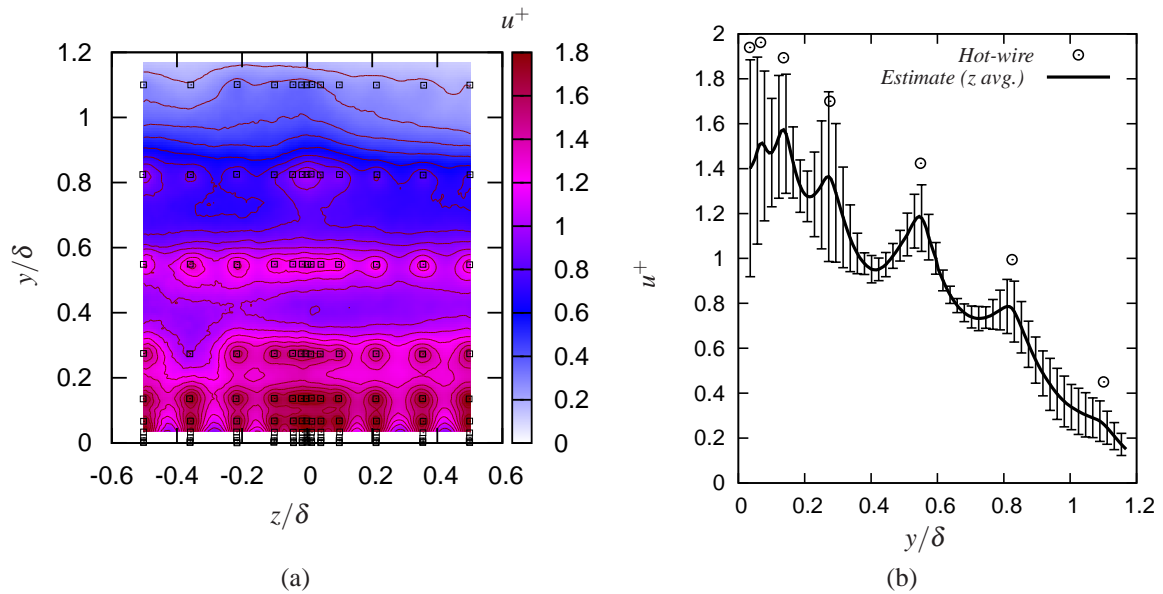


Figure 4. (a) Map of u^+ levels obtained for the conditional estimated field. (b) Spanwise averaging of u^+ shown in (a) compared to that measured by the hot-wire sensors. The errorbars gives the extrema estimated along the spanwise direction.

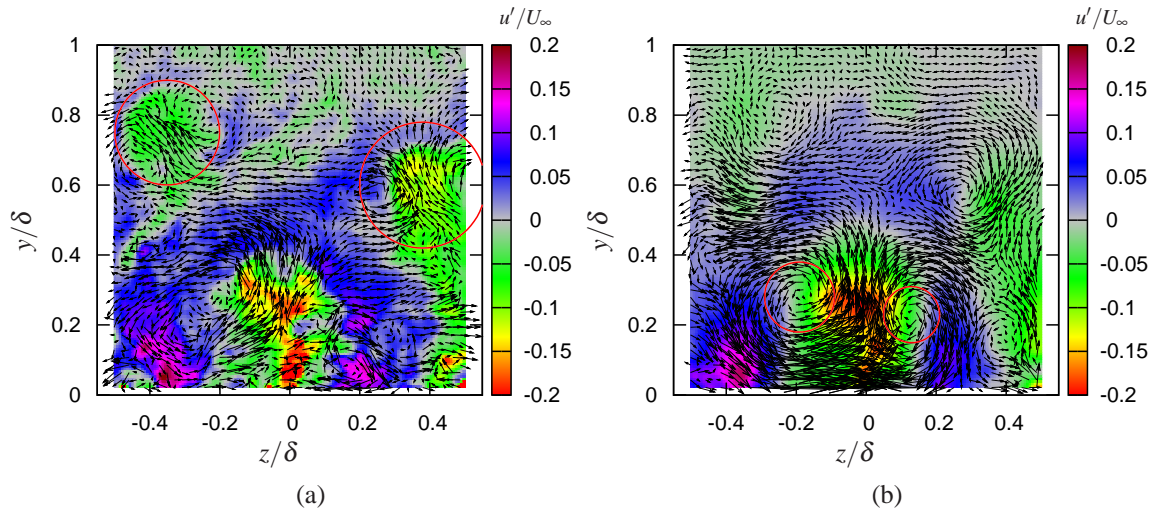


Figure 5. Snapshot of the 3D velocity fluctuations in the $(y-z)$ plane from (a) original PIV measurements, (b) conditional estimates. The colormap gives the amplitude of the streamwise fluctuations while the other components are given by the vector arrows. The red circles indicate location of rotating events. To help for the visualisation, a factor of 5 is used in (b) for the velocity vectors.

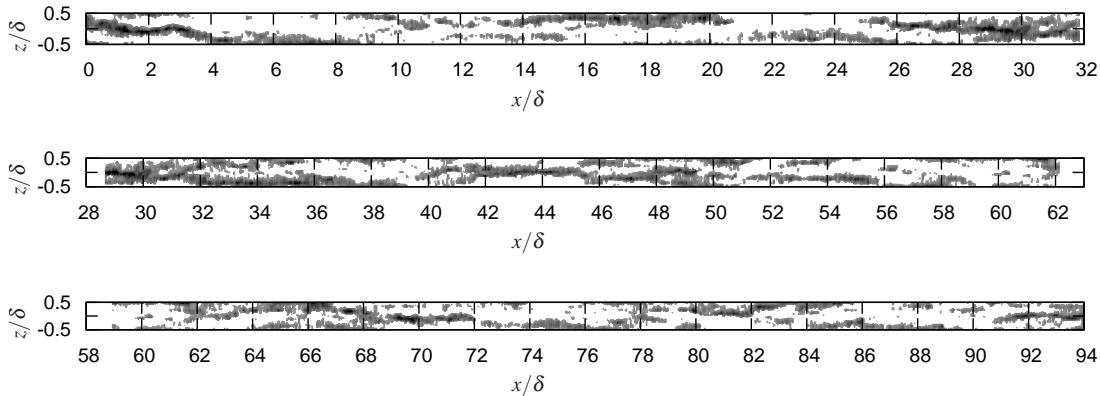


Figure 6. Reconstructed streamwise low-speed fluctuations $u'/U_\infty < -0.15$ in a plane parallel to the wall located at $y^+ = 361$ using the Taylor's hypothesis with free flow velocity.

scales, also illustrating the high spatial resolution of the PIV data. In the outer part of the boundary layer close to its vicinity, mushroom-like events are identified (highlighted by the circles) with counter-rotating vortices well captured. These are typical event observed in the border of the boundary layer with the free flow. Closer to the wall, while fluid events with larger absolute fluctuations are observed, it is more difficult to discern any events with well defined pattern.

The conditional estimate of the same field at the same instant is shown in figure 5(b). When examining first the streamwise component, the overall structure of the original PIV field is well recovered. The low-pass filtering is manifest. The mushroom-like events identified in the original field are somehow modified. Closer to the wall, a low-speed fluid region ($u' < 0$) surrounded by high-speed fluid ($u' > 0$) and a pair of counter-rotating vortices (highlighted by the red circles) is now identifiable in a region where a wider range of scales is observable in the original PIV data. This event corresponds to low-speed fluid being ejected from the wall with the presence of two counter-vortices on both side of it: this has the expected topology of a low-speed super-

streak, such as described by Adrian (2007) among others, and which is difficult to identify in the original PIV data of figure 5(a) due to the blurring by smaller scales. Close examination of successive snapshots reveal that the identified low speed regions remain persistent and relatively well localised. Due to the high temporal resolution of the estimated field, the velocity fluctuations in the streamwise direction can be approximated using the Taylor's hypothesis. For simplicity, the velocity of the free flow is used as convection velocity. This allows reconstruction of the velocity fluctuations to be observed in a $x-z$ plane parallel to the wall such as depicted in figure 6. The plane is here located at $y^+ = 361$ ($y/\delta = 0.1$) from the wall which roughly corresponds to the region where maxima of low-speed fluctuations are observed in figure 5(b). In figure 6, only levels of fluctuations $u'/U_\infty < -0.15$ are shown for sake of clarity. Streamwise extended structures are found with an average extend of about 10δ . This is consistent with previous findings in the literature regarding the lifetime of these structures (Carlier & Stanislas, 2005; Ganapathisubramani *et al.*, 2012). Such entities could not have been observed with classical PIV systems. The methodology developed

August 28 - 30, 2013 Poitiers, France

therefore offers the potential for capturing such structures with perspective to better understand their role in dynamics of flow.

The two counter-rotating vortices identified previously remain also well persistent while the low-speed fluid region exists. Samples of snapshots are reported in figure 7 for different time steps. These have been extracted from long reconstructed time sequence. The relative position of the two vortices significantly changes with time but remains well attached to the low speed streak. These may be associated to the legs of a large hairpin vortex sitting on the streak such as described by Adrian (2007) for example. Here again, the methodology proposed offers the potential for extraction of these entities which are known to play an active role in the dynamics of the boundary layer. While extraction of such structures is out of the scope of the present paper, the reconstructed data constitutes a valuable database for future work in the understanding of turbulence regeneration in boundary layers.

Conclusion

Time-resolved estimate of high spatially-resolved PIV data, initially sampled at 4 Hz, in a wall-normal plane of a turbulent boundary layer is effected by means of linear stochastic estimation. Streamwise velocity fluctuations recorded by a two-dimensional rake of single hot-wire probes located downstream of the PIV plane are used as observers. The current paper shows the potential of the methodology proposed for eduction of large scale structures and offers the opportunity for a deep examination of their organisation.

Acknowledgments

The present research work was supported by International Campus on Safety and Intermodality in Transportation the Nord-Pas-de-Calais Region, the European Community, the Regional Delegation for Research and Technology, the Ministry of Higher Education and Research, and the National Center for Scientific Research.

REFERENCES

Adrian, R.J. 1994 Stochastic estimation of the structure of turbulent fields. *Lectures on Stochastic Estimation, Int. Center for Mech. Sc., May 23–27, Udine (Italy)*.

Adrian, R.J. 2007 Hairpin vortex organization in wall turbulence. *Phys. Fluids* p. 041301.

Adrian, R.J., Meinhart, C.D. & Tomkins, C.D. 2000 Vortex organisation in the outer region of the turbulent boundary layer. *J. Fluid Mech.* **422**, 1–54.

Adrian, R.J. & Moin, P. 1988 Stochastic estimation of organized turbulent structure- homogeneous shear flow. *J. Fluid Mech.* **190** (1), 531–559.

Blackwelder, R.F. & Kaplan, R.E. 1976 On the wall structure of the turbulent boundary layer. *J. Fluid Mech.* **76** (1), 89–112.

Blackwelder, R.F. & Kovaszny, L.S.G. 1972 Large-scale motion of a turbulent boundary layer during relaminarization. *J. Fluid Mech* **53** (Part 1), 61–83.

Carlier, J. & Stanislas, M. 2005 Experimental study of eddy structures in a turbulent boundary layer using particle image velocimetry. *J. Fluid Mech.* **535** (36), 143–188.

Christensen, K.T. & Adrian, R.J. 2001 Statistical evidence of hairpin vortex packets in wall turbulence. *J. Fluid Mech.* **431**, 433–443.

Cordier, L., Abou El Majd, B. & Favier, J. 2010 Calibration of POD reduced-order models using tikhonov regularization. *Int. J. Num. Meth. in Fluids* **63** (2), 269–296.

Coudert, S., Foucaut, J.M., Kostas, J., Stanislas, M., Braud, P., Fourment, C., Delville, J., Tutkun, M., Mehdi, F., Johansson, P. & George, W.K. 2011 Double large field stereoscopic piv in a high reynolds number turbulent boundary layer. *Exp. Fluids* **50**(1), 1–12.

Delville, J., Braud, P., Coudert, S., Foucaut, J.M., Fourment, C., George, W.K., Johansson, P.B.V., Kostas, J., Mehdi, F., Royer, A. *et al.* 2010 The wallturb joined experiment to assess the large scale structures in a high reynolds number turbulent boundary layer. In *Progress in Wall Turbulence: Understanding and Modeling: Proceedings of the WALLTURB International Workshop Held in Lille, France, April 21-23, 2009*, vol. 14, p. 65. Springer Verlag.

Foucaut, J.M., Coudert, S., Stanislas, M., Delville, J., Tutkun, M. & George, W.K. 2010 Spatial correlation from the spiv database of the wallturb experiment. *Progress in wall turbulence: understanding and modelling, ERCOFTAC Series*.

Ganapathisubramani, B., Hutchins, N., Monty, J.P., Chung, D. & Marusic, I. 2012 Amplitude and frequency modulation in wall turbulence. *J. Fluid Mech.* **709**.

Graftieaux, L., Michard, M. & Grosjean, N. 2001 Combining PIV, POD and vortex identification algorithms for the study of unsteady turbulent swirling flows. *Meas. Sci. Technol.* **12**, 1422–1429.

Hamilton, J.M., Kim, J. & Waleffe, F. 1995 Regeneration mechanisms of near-wall turbulence structures. *J. Fluid Mech.* **287** (1), 317–348.

Kerhervé, F., Jordan, P., Cavalieri, A.V.G., Delville, J., Bogy, C. & Juvé, D. 2012 Educting the source mechanism associated with downstream radiation in subsonic jets. *J. Fluid Mech.* **710**, 606–640.

Kline, S.J., Reynolds, W.C., Schraub, F.A. & Runstadler, P.W. 1967 The structure of turbulent boundary layers. *J. Fluid Mech.* **30**, 741–773.

Kovaszny, L.S.G., Kibens, V. & Blackwelder, R.F. 1970 Large-scale motion in the intermittent region of a turbulent boundary layer. *Journal of Fluid Mechanics* **41** (02), 283–325.

Mathis, R., Hutchins, N. & Marusic, I. 2011 A predictive inner-outer model for streamwise turbulence statistics in wall-bounded flows. *J. Fluid Mech.* **681**, 537–566.

Robinson, S.K. 1991 Coherent motions in the turbulent boundary layer. *Ann. Rev. Fluid Mech.* **23**, 601–639.

Sirovich, L. 1989 Chaotic dynamics of coherent structures. *Physica D* **37**, 126–145.

Smith, C.R. & Metzler, S.P. 1983 The characteristics of low-speed streaks in the near-wall region of a turbulent boundary layer. *J. Fluid Mech.* **129** (1), 27–54.

Smits, A.J., McKeon, B.J. & Marusic, I. 2011 High-reynolds number wall turbulence. *Ann. Rev. Fluid Mech.* **43**, 353–375.

Stanislas, M., Jimenez, J. & Marusic, I. 2009 Progress in wall turbulence: understanding and modelling. In *Proc. WALLTURB Int. Workshop held in Lille, France, April 21-23*.

Stanislas, M., Perret, L. & Foucaut, J.M. 2008 Vortical structures in the turbulent boundary layer: a possible

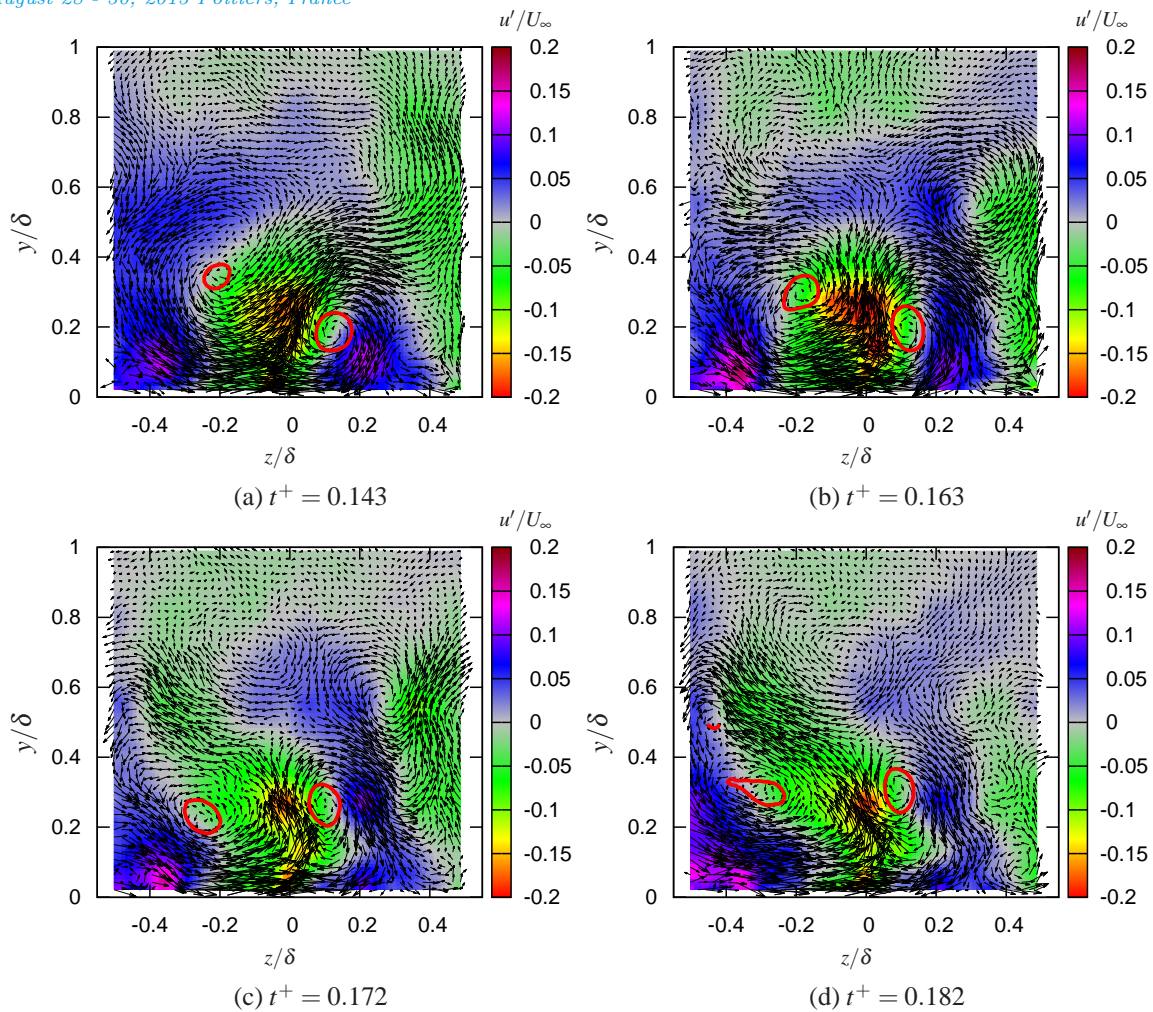


Figure 7. Conditional estimated field at different time steps. The red contours highlight center of vortical structures identified by the criteria of Graftieux *et al.* (2001) around the low-speed streak of interest.

route to universal representation. *J. Fluid Mech.* **602**, 327–382.

Theodorsen, T. 1952 Mechanism of turbulence. *Proc. 2nd Midwestern Conf. on Fluid Mechanics* pp. 1–19.

Tomkins, C.D. & Adrian, R.J. 2003 Spanwise structure and scale growth in turbulent boundary layers. *J. Fluid Mech.* **490**, 37–74.

Townsend, A. 1976 The structure of turbulent shear flow. *2nd Edn. Cambridge University*.

Tutkun, M., George, W.K., Delville, J., Stanislas, M., Johansson, P.B.V., Foucaut, J.M. & Coudert, S. 2009a Two-point correlations in high Reynolds number flat plate turbulent boundary layers. *J. Turbulence* (10).

Tutkun, M., George, W.K., Foucaut, J.M., Coudert, S., Stanislas, M. & Delville, J. 2009b In situ calibration of hot wire probes in turbulent flows. *Exp. Fluids* (46(4)), 617–629.